Available online at www.sciencedirect.com

SciVerse ScienceDirect

Procedia CIRP 8 (2013) 322 – 327

www.elsevier.com/locate/procedia

14th CIRP Conference on Modeling of Machining Operations (CIRP CMMO)

Simulation of Hexa-Octahedral Diamond Grain Cutting Tests Using the SPH Method

N. Rüttimann[a]*, M. Roethlin[a], S. Buhl[b], K. Wegener[a]

[a]*Institute of Machine Tools and Manufacturing, ETH, CLA Tannenstrasse 3, 8092 Zürich, Switzerland*
[b]*Inspire AG, CLA Tannenstrasse 3, 8092 Zürich, Switzerland*
* Corresponding author. Tel.: +41-44-632-8217 ; fax: +41-44-632-1159 .*E-mail address*: ruettimann@iwf.mavt.ethz.ch.

Abstract

Single grain cutting tests are an important basic tool in understanding complex grinding processes. Simulations offer additional insight into important process data and can reduce the overall number of required experiments.
Cutting simulations with FE Methods have problems arising from large deformations at the chip root and negative rake angles of the diamond grain. Those problems can be overcome using meshfree methods, but with the additional difficulties of contact modeling and the enforcement of boundary conditions. In this work, a Smoothed Particle Hydrodynamics (SPH) Method is used to model the cutting behavior of single hexa-octahedral diamond cutting grains. The material behavior at low cutting depths is characterized using experimental data and simulations of micro-Vickers indenter tests.
The simulations show the influence of the yaw and rake angle on the cutting and passive forces as well as the ratio of chip and burr generation. Both the cutting and the passive forces show good accordance with the experimental data. The burr generation is still overestimated due to the lack of a physical failure criterion in the SPH-method. Difficult to predict effects like the generation of a stagnant zone of workpiece material moving in front of the diamond grain at the chip root are reproduced as well. This work shows the advantages of using a meshfree method in areas were classical FE-methods have difficulties.

Selection and peer-review under responsibility of The International Scientific Committee of the "14th CIRP Conference on Modeling of Machining Operations" in the person of the Conference Chair Prof. Luca Settineri

Keywords: SPH; Grinding; Single Grain Cutting;

1. Introduction

Grinding constitutes an important machining process for finishing and high precision machining processes. The prediction of the process results hinges on the ability to model the material removal process, which can be seen as a combination of superimposed single grain cutting processes. The understanding of the mechanics of the single grain cutting process is therefore critical in the further developments of grinding processes. This is especially critical in the development of Engineered Grinding Tools (EGT), which feature a defined pattern of a small number of grains placed on the grinding tool [1]. These patterns have higher cutting depths per grain and experience therefore a higher mechanical and thermal load during cutting.

The simulation of the material removal process of a complete grinding wheel is problematic with current finite element (FE) methods. The stochastic surface of the grinding tool coupled with the length scale ratio between the tool dimensions and the cutting depths between 0.1 and 20 µm make complete tool simulations computationally too expensive to remain feasible.

Single grain cutting simulations are possible using FEM, but are computationally expensive, especially in fully three dimensional models. In order to avoid these problems, a meshfree Smoothed Particle Hydrodynamics (SPH) method is employed to simulate these cutting tests.

1.1. Modeling of single grain cutting operations

An overview over grinding and micro-scale single grain modeling and simulation can be found in [2], with

Selection and peer-review under responsibility of The International Scientific Committee of the "14th CIRP Conference on Modeling of Machining Operations" in the person of the Conference Chair Prof. Luca Settineri
doi:10.1016/j.procir.2013.06.110

newer developments found in [3] and [4]. Even at the micro-scale, most models have been restricted to two-dimensional models, like those presented in [2], brittle materials in [5] or the rubbing and ploughing phases in [3] and [6], where no chip generation takes place.

These simplified models are necessary due to the high computational cost and the problems of FE-methods in handling the changing mesh topography caused by material separation and large deformations in the shear zone. This problem is especially pronounced in single grain cutting tests that feature large negative rake angles and complex material flow patterns around the cutting edge [7].

Three dimensional chip generation models are comparatively few due to the high computational demands, such as Yan et al. [8], Hoffmeister and Gerdes [9] and Huang et al. [10].

1.2. Smoothed Particle Hydrodynamics

The SPH method, developed by Lucy [11], Monaghan and Gingold [12] is the original method of a family of discretization methods commonly referred to as meshfree, meshless or particle methods [13]. The method has already been used in publications of metal cutting processes with defined cutting geometries, for instance by Limido et al. [15] and Villumsen and Fauerholdt [16]. Also, newer methods are under development for application in metal cutting problems, for instance by Uhlmann et al. [17].

Meshfree methods differ from FE-methods in the employed discretization and the construction of the shape function. The continuum is discretized with a cloud of nodes instead of the element mesh of FE-methods. The nodal connectivity is defined by a circular domain called support domain where the neighboring nodes contribute to the field value approximation according to equation (1):

$$\tilde{f}(x_i) \cong \sum_{j=1}^{N} \frac{m_j}{\rho_j} f(x_j) W(x_i - x_j, h) \qquad (1)$$

Where $\tilde{f}(x_i)$ is the function value to be approximated at point i, $f(x_j)$ are N functional values in the support domain at the points j, m_j and ρ_j are the nodal masses and densities, and $W(x_i\text{-}x_j,h)$ is the distance dependent shape function of the form $W(x_i\text{-}x_j,h) = h(u)^{-d}\theta(u)$, where d is the dimension, $u = x_i\text{-}x_j$ and $\theta(u)$ takes the form of a cubic spline function, as shown in equation 2. Using this approach, the governing equations can be formulated in the SPH formalism. For the detailed deduction, the reader is referred to [13] and [14].

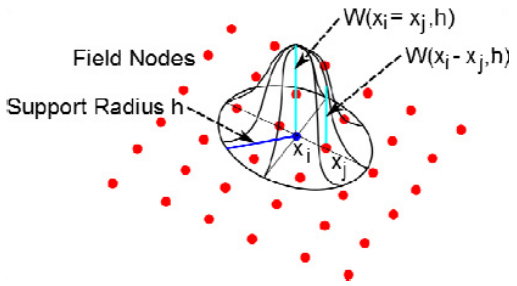

Fig. 1. SPH discretization

SPH circumvents the problems of mesh distortion, as the deformation metric is defined only on one node, and the material separation can be modeled by simply moving the nodes out of mutual support radius without the use of an explicit failure criterion.

These properties make the use of SPH in complex three-dimensional single grain cutting simulations advantageous. Based on preliminary results presented in [18] and the aforementioned publications for machining using defined cutting geometries, the method has been shown to be sufficiently robust for cutting simulations, although the numerical stability is not universally guaranteed [13] and care has to be taken to ensure stability by adapting model parameters like the time step size and artificial viscosity to the simulated properties. Wang et al. also presented comparisons between FE and SPH simulations in [19].

In this work, the SPH implementation in LS-DYNA with a total lagrangian formulation has been used.

$$\theta(u) = C \times \begin{cases} 1 - \frac{3}{2}u^2 + \frac{3}{4}u^3 & \text{for } u \le 1 \\ \frac{1}{4}\left(2 - u^3\right) & \text{for } 1 \le u \le 2 \\ 0 & \text{for } u > 2 \end{cases} \qquad (2)$$

2. Experimental background

2.1. Single grain cutting tests

For the experimental part a single diamond grain is brazed onto a steel pin which is mounted on the spindle of a milling machine, as shown in figure 2. The pin is then moved across the workpiece mounted on the machine table at a cutting speed of 0.18 m/s. Instead of being fully even, the workpiece was slightly tilted, which in turn led to a gradual increase in cutting depth and therefore also in cutting force. This allows for a simple variation of cutting depths, which would otherwise not be available in the necessary precision on the test setup. The matching of the process force to the

cutting depth is performed in the post-experimental analysis.

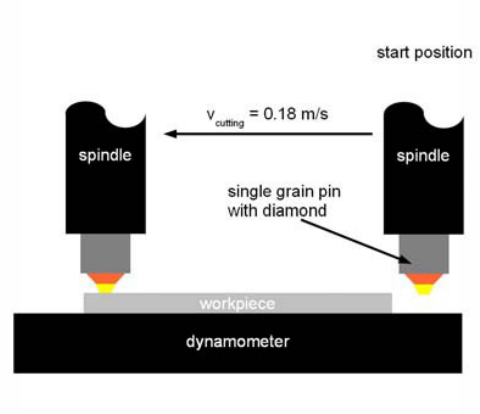

Fig. 2. Experimental Setup

2.2. Measurement equipment

The process forces during the cutting motion were recorded with a Kistler MiniDyn 9246C1 dynamometer. The cutting groove topography was analyzed by recording the workpiece surface using a Zygo NV5000 white-light interferometry microscope to calculate the groove width and depth. From the raw surface data, the averaged cutting depth was isolated and matched to the cutting force signals.

3. Material modeling and simulation setup

In these simulations, a measured hexa-octahedral grain was simulated at cutting depths from 8 to 14 µm and at yaw angles ψ of 0, 22.5 and 45° to analyze its cutting behavior. A real geometry instead of an ideally shaped diamond grain should achieve a better accordance with the measured process properties.

3.1. Model setup

The set-up of the cutting tests presented a design challenge in the form of the ratio of the involved length scales; the edges of the diamond are 30 to 50 times longer than the depth of cut of 0.5 to 10 µm. For a faithful representation of the problem geometry, one has either to generate a huge amount of nodes or decrease the node density and thereby the accuracy or scale the problem geometry. Due to the linear dependence of cutting force to chip width, a scaling of the diamond geometry perpendicular to the cutting direction has been chosen. In this case, the diamond edges are scaled down by a factor of 10 to achieve a diamond side length of 30 µm.

The workpiece is modeled with a length L_{WP} of 0.4 mm, a height H_{WP} of 0.03mm and a width W_{WP} of 0.2 mm. The work piece is discretized with a nodal density of $64*10^6$ nodes/cm^3. The cutting depth D is chosen in the range of 10 µm, according to the measured cutting depths. The simulation setup can be seen in figure 3.

Contact between the SPH nodes of the workpiece and FE the grain was detected based on a node-to-surface contact search algorithm. The friction was modeled using a standard Coulomb law. The friction coefficient µ was measured as 0.3 in standard pin-on-disk tribometer tests.

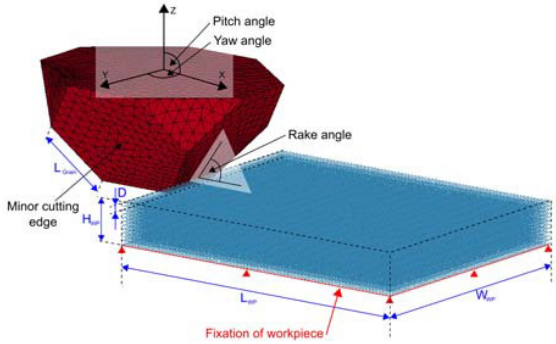

Fig. 3. Model Setup

3.2. Diamond grain geometry

As the geometry of real hexa-octahedral diamond grains differs from the ideal crystal from, the grains were measured on an Alicona InfiniteFocus Real 3D. The corner coordinates in the workpiece plane were measured and used to define the diamond grain. The flank face of the diamond was assumed to be parallel to the workpiece surface. In order to achieve a clear surface definition, the grain was discretized with FE-elements.

3.3. Material modeling

The particular problem of predicting the material behavior in single grain cutting tests is due to the size effect, which plays an important role in the cutting process of both conventional grinding and engineered grinding tools. This size effect is observed when the depth of cut is reduced, leading to a nonlinear increase of the cutting forces, so that approximations like the Kienzle equation can only be fitted locally.

As an overall treatment of the size effect was not in the focus of this work, complex approaches, for example the thermal activation energy model by Weber et al. [20], were not implemented.

Instead a standard Johnson-Cook Material Model [21], as shown in equation (3), was used with parameters that were fitted to the scale of cutting depths of 10 µm.

$$\sigma_y = \left(A + B \cdot \bar{\varepsilon}_{pl}^{n}\right) \cdot \left(1 + C \cdot \ln\left(\frac{\dot{\bar{\varepsilon}}}{\dot{\bar{\varepsilon}}_0}\right)\right) \quad (3)$$

This parameter fitting was performed with a combination of literature data, Vickers indenter tests and indenter simulations to identify these parameters.

As a starting point, material parameters were adapted from [20]. These parameters proved unsuitable, as the cutting forces were underestimated by 70%. To improve the material model, micro hardness tests using a Vickers indentation setup were performed. The indentation test was then simulated using an ALE Model, as shown in figure 4. The material parameters were varied to bring the simulated and real indentation tests into agreement.

The optimization criterion used was the averaged difference between the experimental and simulated indentation force in dependence of time. Test simulations of the single grain cutting test showed a good agreement with the measured force data.

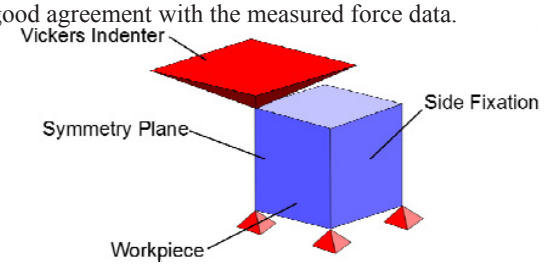

Fig. 4. Vickers Hardness Simulation

The diamond was modeled as rigid, as this saves significant calculation time and the high hardness and Young's modulus of the diamond compared to the workpiece minimizes the diamond deformation at any rate. The elastic material parameters are only used in the calculation of the contact stiffness.

The resulting workpiece material parameters are shown in Table 1.

Table 1. Material Properties of 90MnCrV8

Parameter	Value	Parameter	Value
E_{steel}	275 GPa	n	0.14
ν_{steel}	0.28	C	0.01
ρ_{steel}	7850 Kg/ m^3	$\dot{\bar{\varepsilon}}_0$	10e-6 Hz
A	4 GPa	E_{Dia}	1060 GPa
B	0.5 GPa	ν_{dia}	0.07
μ	0.3	ρ_{dia}	3500 Kg/m^3

4. Simulation Results

A range of different grain orientations and cutting depths was simulated, with computation times of 10 CPU-hours, depending on workpiece size and discretization. This represents a significant speed-up in comparison to the FE-tools available at the institute.

4.1. Process forces

The simulated process forces were scaled up with the same factor used to reduce the diamond grain size. The process forces were in good agreement with the measured forces, as shown in tables 2 and 3. The average error over all simulated cases was 13.52 % for the cutting force and 14.25% for the passive force, with outliers for both the cutting and process forces distorting this result. The cutting forces showed a trend for underestimating the cutting force at a yaw angle of 45° and overestimating it for lower yaw angles. This is probably linked to the occurrence of stagnant zones as outlined in section 4.4 These zones are absent in the case of high yaw angles, which reduces the cutting force acting on the diamond grain.

Table 2. Simulated and Experimental Cutting Forces

D [µm]	ψ [°]	Exp. Fc [N]	Sim. Fc [N]	Err [%]
11	0	8.92	9.88	10.74
13.1	0	11.05	11.78	6.57
8.5	22.5	6.29	7.29	15.97
8.9	22.5	7.59	7.66	0.96
10.1	22.5	7.65	8.75	14.33
13.1	22.5	10.26	11.28	9.90
8.2	45	9.23	6.84	-25.87
8.8	45	8.55	7.39	-13.57
11.7	45	11.80	9.92	-15.92

Table 3. Simulated and Experimental Passive Forces

D [µm]	ψ [°]	Exp. Fp [N]	Sim. Fp [N]	Err [%]
11	0	10.46	8.74	-16.46
13.1	0	11.88	9.77	-17.76
8.5	22.5	7.70	5.37	-30.24
8.9	22.5	8.41	7.54	-10.30
10.1	22.5	8.84	6.89	-22.05
13.1	22.5	11.70	10.26	-12.32
8.2	45	7.67	8.77	14.28
8.8	45	8.50	8.31	-2.21
11.7	45	11.21	11.51	2.65

The passive forces were generally underestimated, which is in line with the current state of the art in metal cutting simulations, though the overall error is smaller. This is supposed to be caused by the 0° clearance angle, which allows for longer contact lengths on the free face and passive forces acting on the cutting faces. Given the general measurement uncertainties, this was deemed a satisfactory result.

4.2. Chip and burr generation

Only a part of the displaced workpiece material is evacuated as a chip. The remaining material is deposited on the sides of the cutting groove and forms a sidewall. A strong dependence on the yaw angle of the grain was visible, as material displaced by a grain surface with a low incident angle relative to the cutting direction tends to deposit the workpiece material as burr, as shown in figure 5. Therefore, a main cutting face with a high incident angle can be defined, which removes material mainly into a chip, and one or several minor cutting faces with high incident angles that primarily produce burrs.

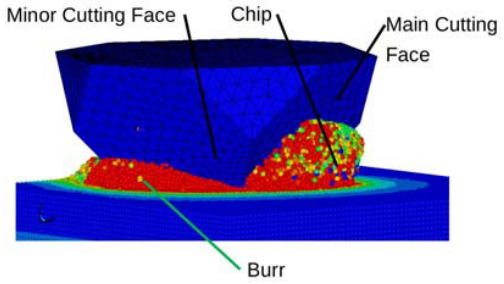

Fig. 5. Chip and Burr Generation

The simulated burr was calculated by using the cumulated mass of the workpiece nodes of the side burrs. As the burr was made up of discrete nodes, no surface area or burr surface coordinates could be calculated to compare the results directly to the measurements.

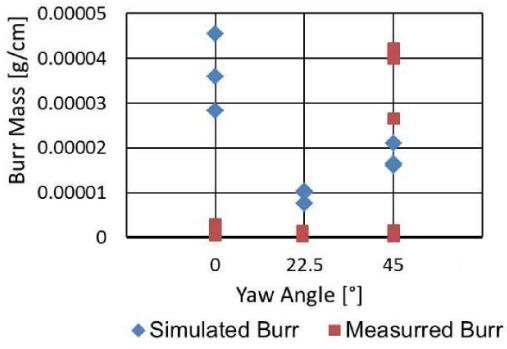

Fig. 6. Simulated and experimental burr generation rate

The simulations showed an ability to reproduce a general trend of a burr mass minimum at 22.5°, but the detailed simulations are not yet in satisfactory accordance with the experiments. This is a direct consequence of the lack of a physical failure criterion in the SPH method, as the burr cannot fail due to accumulated damage or bending, as failure is algorithmically determined by the nodal distances and not physical damage properties.

4.3. Stagnant Zones

Under large negative rake angles it can be observed, that workpiece material at the chip root is not evacuated as chip or pressed below the cutting grain but rather moves in front of the cutting geometry and forms in effect a new cutting geometry, as shown in figure 7. This work-hardened material has been labeled „dead zone" or "stagnant zone" in [22] and [23].

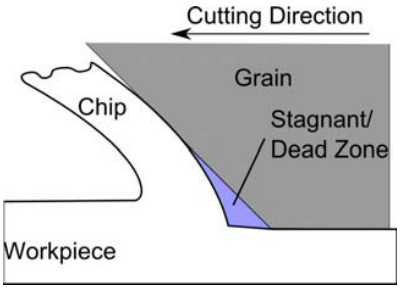

Fig. 7. Stagnant zones, from [23]

This dead zone is detectable in the SPH simulations, as this simulation shows a mass of SPH particles featuring high plastic strains which moves with the diamond grain at the height of the chip root, as illustrated in figure 8.

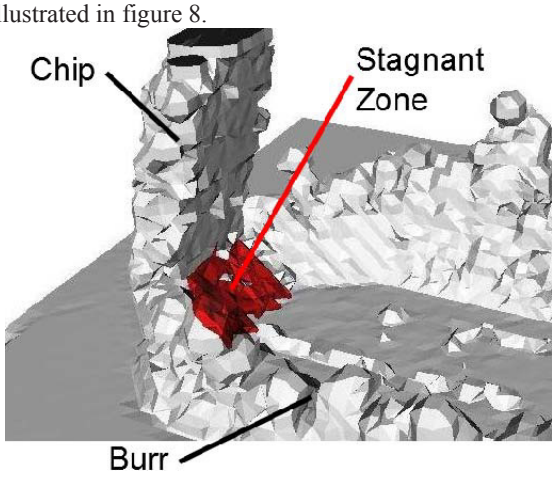

Fig. 8. Stagnant zones in SPH simulation

This zone shows an increased equivalent plastic strain above 4.0, compared to the chip which features plastic strains in the range from 2-4.0. This is caused by the long duration of compressive stress enacted from both the grain and the surrounding workpiece material during cutting. This zone is identified using a combination the

plastic strain above 4.0 and a particle speed +/- 10% of the grain speed.

5. Conclusion and outlook

The results of this work can be summarized as follows:

1) The use of a Vickers indenter test and indenter simulations to adapt the material properties to very low cutting depths yielded satisfactory results, although the fitted parameters are only valid for the employed indenter and cutting depths.
2) The process forces were predicted in a reasonable accuracy given measurement and model uncertainties.
3) The SPH method was able to reproduce stagnant zones in agreement to results reported in literature and observed qualitatively in the experiment.
4) The burr prediction is not yet satisfactory and needs further development in the SPH formulation.

Future research will concentrate on measuring the properties of the stagnant zones and develop material models to predict its influence on the process forces and the surface integrity.

A second focus will be the improvement of the burr prediction with the inclusion of material failure models and failure handling algorithms for the SPH model, which allow physics-based models of the burr breakage.

References

[1] Pinto, F. W., Vargas, G. E. & Wegener, K., 2008. Simulation For Optimizing Grain Pattern On Engineered Grinding Tools, Annals of the CIRP 57/2, p. 353.

[2] Doman, D. A., Warkentin, A. & Bauer, R., 2009. Finite Element Modeling Approaches In Grinding. International Journal of Machine Tools and Manufacture 49, p.109.

[3] Opoz, T. T., Chen, X., 2010. "Numerical Simulation of Single Grit Grinding", Proceeding of the 16th International Conference on Automation & Computing. Birmingham, UK.

[4] Park, H. W., Liang, S. Y., 2009. Force Modeling Of Microscale Grinding Process Incorporating Thermal Effects, The International Journal of Advanced Manufacturing Technology 44, p. 476.

[5] Zhang, B., Peng, X., 2000. Grinding Damage Prediction For Ceramics Via CDM Model, Journal of Manufacturing Science and Engineering 122, p.51.

[6] Doman, D. A., 2008. Rubbing And Plowing Phases In Single Grain Grinding, PhD Dissertation, Dalhousie University.

[7] Abebe, M., Appl, F., 1988. Theoretical Analysis Of The Basic Mechanics Of Abrasive Processes, Wear 126, p. 251.

[8] Yan, L., Zhou, Z. Jiang, F., Li, X.K., Rong, Y., 2010. Grain-Workpiece Interaction Study of Grinding Process through Single Grain Cutting Simulation, Key Engineering Materials 431, p. 269.

[9] Hoffmeister, H. W., Gerdes, A., 2011. Finite Element Simulation of Quick-Stop Experiments for Better Understanding of Chip Formation in Grinding, Advanced Materials Research 223, p. 764.

[10] Huang, C., Zhu, H., Wang, J., Li, X., 2012. Grinding Surface Creation Simulation Using Finite Element Method and Molecular Dynamics, Advanced Materials Research 500, p. 314.

[11] Lucy, L.B., 1977. A Numerical Approach To The Testing Of The Fission Hypothesis, The Astronomical Journal 82, p. 1013.

[12] Monaghan, J.J., Gingold, R.A., 1977. Smoothed Particle Hydrodynamics - Theory And Application To Non-Spherical Stars, Royal Astronomical Society 181, p. 543.

[13] Liu, G.R., Liu, M.B., 2003. Smoothed Particle Hydrodynamics - A Meshfree Particle Method, World Scientific Publishing.

[14] Hallquist, J.O., 2006. LS-DYNA Theory Manual, LSTC.

[15] Limido, J., Espinosa, C., Salaun, M., Lacome, J.P., 2006. A New Approach Of High Speed Cutting Modelling: SPH Meth-od, Journal de Physique IV 134, p. 1195.

[16] Villumsen, M.F., Fauerholdt T. G., 2008. Simulation Of Metal Cutting Using Smooth Particle Hydrodynamics, 7. LS-DYNA Anwenderforum, C-III, p. 17.

[17] Uhlmann, E., Gerstenberger, R., Graf von der Schulenburg, M., Kuhnert, J., Mattes, A., 2009. The Finite-Pointset-Method for the Meshfree Numerical Simulation of Chip Formation. Proceedings of the 12th CIRP Conference on Modeling of Machining Operations 1, p. 145.

[18] Rüttimann, N., Buhl, S., Wegener, K., 2010. Simulation of Single Grain Cutting Using SPH Method, Journal of Machine Engineering 10, p. 17.

[19] Guan, P., Li, J.Q., Zhu, S., Yu, T.B., Wang, W.S., 2012. Advances in Simulation of Grinding Process, Applied Mechanics and Materials 121, p. 1879.

[20] Weber, M. et al., 2007. Investigation of Size-effects in Machining with Geometrically Defined Cutting Edges. Machining Science and Technology 11, p. 447.

[21] Johnson, G.R., Cook, W.H., 1985. Fracture Characteristics of Three Metals Subjected to Various Strains, Strain Rates, Temperatures and Pressures. Engineering Fracture Mechanics 21, p. 33.

[22] Ohbuchi, Y., Obikawa, T., 2003. Finite Element Modeling Of Chip Formation In The Domain Of Negative Rake Angle Cutting, Journal of engineering materials and technology 125, p. 324.

[23] Ohbuchi, Y., Obikawa, T., 2005. Adiabatic Shear In Chip Formation With Negative Rake Angle, International Journal of Mechanical Sciences 47, p. 1377.